A spectral analysis of ground-penetrating radar data for the assessment of the railway ballast geometric properties

A spectral analysis of ground-penetrating radar data for the assessment of the railway ballast geometric properties

Luca BIANCHINI CIAMPOLI[1], Fabio TOSTI[2]*, Maria Giulia BRANCADORO[1], Fabrizio D'AMICO[1], Amir M. ALANI[2], Andrea BENEDETTO[1]

[1]Department of Engineering, Roma Tre University, Via Vito Volterra 62, 00146, Rome, Italy
e-mail: luca.bianchiniciampoli@uniroma3.it; fabrizio.damico@uniroma3.it; mariagiulia.brancadoro@uniroma3.it; andrea.benedetto@uniroma3.it

[2]School of Computing and Engineering, University of West London (UWL), St Mary's Road, Ealing, London W5 5RF, UK e-mail: Fabio.Tosti@uwl.ac.uk (*Corresponding author); Amir.Alani@uwl.ac.uk

Abstract

This paper presents a methodology for the assessment of railway ballast using ground-penetrating radar (GPR – 2 GHz horn antenna). The primary approach in this endeavour was the finite-difference time-domain (FDTD) simulations of ballast (a multi-stage process in terms of ballast size). To this effect, a combination of random-sequential adsorption (RSA) and FDTD algorithms were applied. The results of the numerical simulation then were used to compare with the experimental investigations results using a container (methacrylate material) of the 1.5×1.5×0.5m dimensions. Finally, the modelling of the frequency spectrum peak and the equivalent diameter of the ballast aggregates was developed.

Keywords: ground-penetrating radar; GPR; railway ballast; grain size; frequency spectral domain; finite-difference time-domain (FDTD) simulation; random-sequential adsorption (RSA) paradigm

1. Introduction

Railways are major transportation assets in sustaining the economy and providing massive transport of public and freight. To tackle the challenge of i) sustaining a growing demand for freight and passengers timely and safely, and ii) competing with other modes of transportation, railway industries are seeking to lower construction and maintenance costs while maintaining high levels of serviceability. To this purpose, the effective management of funds allocation (proper maintenance of the railways) and the efficient inspection of rail networks are factors of paramount importance.

Within the railway construction types, the ballasted rail tracks are the most widespread since they allow for the effective drainage of the track-bed and provide proper load-bearing capacity at relatively low costs. From a structural point of view, a track structure is composed of a superstructure (steel rails, fastening systems and concrete/timber sleepers) laying over a substructure (ballast, subballast and subgrade). The cyclic loading exerted by the moving trains affects the structural stability of these two components, although major deformations occur mostly in the ballast and subballast layers. Thereby, the proper selection and the effective monitoring of the ballast aggregates in the construction and maintenance stages are critical factors. This is due to the progressive deterioration and segregation of the aggregates under heavy cyclic loading [1].

The railway ballast layer usually consists of uniformly-graded coarse aggregates produced from crushed rocks such as granite, basalt, limestone or gravel. The major structural and functional tasks of the ballast aggregates are i) to resist to the vertical, lateral and longitudinal forces applied to the sleepers, ii) lowering the pressure from the sleeper-bearing area to minor stress levels for the underlying material and iii) providing effective water drainage [2]. Differential railway track settlements with implications on the operational safety of the infrastructure can be due to the combination of several critical factors, such as the number and the amplitude of the load cycles, the track confining stress, the aggregates grading, the angularity and the fracture strength of the grains. The track stability is also widely affected by the ballast fouling, which is broadly related to the breakdown of the ballast aggregates and the infiltration of external materials from the ballast surface or from the base of the ballast layer. Nevertheless, the most important source of fouling reported worldwide is related to the segregation of the ballast aggregates (i.e., the formation of smaller ballast aggregates) [2]. In view of this, the effective monitoring and detection of “critical” geometric features of the aggregates, such as the grain size characteristics, are necessary to ensure the optimum maintenance of the rail infrastructure. These actions

contribute to preserving the structural stability of the rail track as well as to maintain proper operational safety conditions.

Drilling and digging trenches at even intervals along the track are widespread methodologies to retrieve physical and geometric information on the railway ballast. Nevertheless, these techniques are intrusive, locally representative of the extensive rail infrastructures and require to constrain the operation of trains. Within this context, non-destructive testing (NDT) techniques are becoming popular in railway engineering. The applications of infrared imaging [3], electrical resistivity tomography [4], seismic surveys [5] and, mostly, ground-penetrating radar (GPR) [6] have increased over the last two decades. According to Roberts et al. [7], first GPR applications in railway engineering date back to the nineteen eighties [8].

The GPR technique is based on the transmission/reception of electromagnetic (EM) waves into the ground in a given frequency band [9]. Inhomogeneities in the materials with different EM properties and interfaces between different structural layers cause changes in the position and the amplitude of the signal peaks. In view of this, information can be inferred about the layer thicknesses and the materials properties (Figure 1). Overall, GPR-based studies on railway ballast can be classified into i) research based on the analysis of the signal response in the time domain and ii) methods based on the analysis of the signal spectrum in the frequency domain.

The earliest and the most tackled GPR investigations on railway ballast are broadly comprised in the first class of research. Within this context, comprehensive analyses of different types of ballast (i.e., mineralogy and grain size) can be found in [10-12]. Usually, the estimation of the permittivity of the substructure layers [13, 14] and the analysis of the signal amplitude variability are performed [15, 16].

On the other hand, the frequency-based analysis (i.e., spectral analysis) of the GPR data was started for railway applications since the second half of the noughties. The main benefit of this approach is that minimum or no destructive sampling is required for the calibration of the system. The time-variation of the frequency spectrum was investigated by Leng and Al-Qadi [17] using the short-time Fourier transform (STSF) approach. The authors demonstrated graphically the variation of the frequency energy with the ballast depth under different fouling conditions. Shao et al. [18] developed an algorithm to extract magnitude spectra at salient frequencies and to classify railway ballast conditions using support vector machines. Xiao and Liu [19] used the forward and the inverse S-transform to 100- and 400-MHz GPR data. The GPR spectra from both the frequencies were

fused together and new spectra with broader bandwidth were derived. In view of this, the authors obtained an effective trade-off between good resolution and deep penetration in ballast surveys. More recently, the finite-difference time-domain (FDTD) simulation of the GPR signal has proved to be an effective technique for the interpretation of complex scenarios in rail substructures and the validation of the above approaches [20-22].

The above-mentioned methodologies demonstrated high reliability and good effectiveness in the ballast health monitoring and fouling detection. Nevertheless, to the best of our knowledge, no studies to date have focused on the assessment of the "critical" geometric features of the ballast aggregates with GPR-based methods implemented in the frequency (spectral) domain of the signal. Liu et al. [22] modelled experimentally and numerically the scattering loss from both rough-surface and subsurface dielectric scatterers. The authors compared the 900-MHz GPR signal amplitude and waveform reflected from the metal sheet at the bottom of a large container (filled with boulders) with the numerically-computed response from a discrete random medium (DRM) model. This model consisted of a collection of densely packed ellipsoids. The diameters of the ellipsoids were accurately measured using the laser scanner technique [23]. The authors analysed the scattering attenuation loss and the velocity dispersion in the time domain of the signal. Apart from this study (developed for rounded boulders in the GPR signal time domain), no research was specifically carried out in the spectral domain of the GPR signal to assess the geometric characteristics of coarse-grained sharp aggregates, such as the railway ballast aggregates.

In view of the above, this study presents a methodology based on the spectral analysis of GPR data collected using a 2GHz horn antenna. A multi-stage process in terms of ballast grain size was developed. FDTD numerical simulations and real tests were both performed to analyse the spectral behaviour of the collected GPR signals. The data from these tests were used for modelling purpose. In this regard, information about relevant geometric features of the railway ballast aggregates was found with respect to the shifting of the frequency spectrum peak.

It is important to emphasize that the methodology aims at providing information of paramount importance about the ballast grain size to the railway network operators. This information is crucial to reduce the railway track-bed maintenance costs and to maintain proper operational safety conditions. The methodology could found effective application in both quality control inspections of newly built infrastructures (i.e., to verify the consistency between the "design" and the "as-built" condition of the aggregates grain size in the ballast and

the subballast layers) as well as in routine maintenance operations (e.g., the monitoring of the segregation processes of the ballast aggregates) in railway engineering.

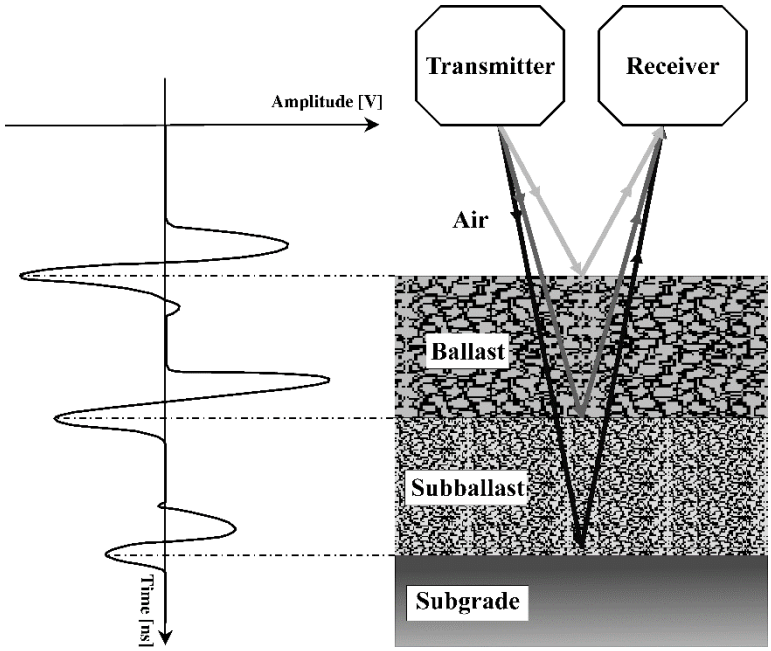

Figure 1. Typical ballasted rail track substructure and corresponding A-scan from a GPR measurement.

2. Objectives and methodology

This paper focuses on the assessment of "critical" geometric features of the ballast aggregates within a railway track-bed. To this purpose, spectral analyses of the 2GHz GPR data were performed in the frequency domain. A bottom-up approach that used simulated and real data collected from laboratory experiments was followed. FDTD simulations with the gprMax 2D numerical simulator [24] were firstly performed. In the first simulation tests, simplified models of mono-sized ballast particles were taken into account. The diameters of the above particles were progressively increased in the range of usage of the ballast aggregates for the construction of railway track-beds. Single- and multi-particle scenarios were simulated and the corresponding frequency spectra of the signals were analysed. Afterwards, the numerical model was rendered more complex by performing real-scale simulations of multi-sized ballast particles. The information on the grain size of these particles was retrieved by the grain size distribution of three typical grading curves used by railway network operators for the construction of ballasted track-beds. The reproduction of the above complex numerical model

was obtained by the combination of the random-sequential adsorption (RSA) paradigm and the FDTD technique.

Real tests were subsequently carried out in the laboratory environment where three different scenarios of the ballast aggregates arrangement were manufactured. Finally, the modelling of the frequency spectrum peak and the equivalent diameter of the ballast aggregates was developed.

The remainder of this paper is organized as follows. In Section 3, the theoretical framework is introduced. In this regard, comparisons between the working principles of analogous electrical and mechanical systems and the "ballast-EM field" interaction (propagation and scattering phenomena of the EM waves within a railway ballast layer) was defined. The numerical simulations are discussed in Section 4, where the outcomes of a multi-stage scenario in terms of ballast size and particles interaction are shown. The laboratory set-up and the main results from the real tests in the laboratory are outlined in Section 5. The discussion of the results and the consistency with the theoretical assumptions are addressed in Section 6. The experimental-based modelling of the spectral behaviour (in both the simulation scenarios and the laboratory experiments) against the relevant geometric features of the ballast aggregates (i.e., the equivalent diameter of the ballast particles) is discussed in Section 7. Finally, conclusions and future perspectives are given in Section 8.

3. Theoretical Framework

In order to investigate the propagation and the scattering of an EM wave through a dielectric medium such as a ballast layer in a railway track-bed, a simplified "analogous" physical model, based on the circuit theory, was proposed to approximate the real system.

It is known that the ballast particles hold an electrical conductivity σ that is dependent on the mineralogy of the source rock. Consequently, an EM wave that propagates through these dielectrics is expected to undergo electrical losses and attenuation. To this effect, a second order model can be used to represent a simple system composed of one ballast grain to which an EM field is applied. This system was streamlined in the analogous electrical circuit showed in the diagram of Figure 2.

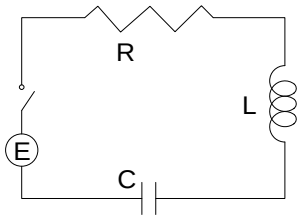

Figure 2. Diagram of the analogous electrical circuit representing one ballast grain to which an EM field is applied.

The system is composed of an electromotive force $E(t)$ applied to a circuit with one resistor R, one inductor L, and one capacitor C, all of which are connected in series. According to the Kirchhoff's voltage law, a second order differential equation, expressing the charge $Q(t)$ that moves into the capacitor, can be derived as follows:

$$L\frac{\partial Q(t)^2}{\partial t^2} + R\frac{\partial Q(t)}{\partial t} + \frac{Q(t)}{C} = E(t) \quad (1)$$

In case of negligible R, the natural pulsation of the system ω_n is given by:

$$\omega_n = 1/\sqrt{LC} \quad (2)$$

When the resistor in no more negligible, the pulsation of the charge in the capacitor and the current in the circuit become:

$$\omega = \omega_n\sqrt{1 - \left(\frac{1}{2F}\right)^2} \quad (3)$$

with F being the quality factor of the circuit that varies with the circuit physical characteristics. In this case, L and C are responsible for storing and freeing the electric and magnetic fields, respectively, whereas R represents the attenuation constant. In such a system, the energy continuously oscillates between the electric and magnetic fields (and vice versa), while getting attenuated by the resistance. In the above framework it is thereby clarified the likeness with the "railway ballast/EM waves propagation" system, where the electric and magnetic fields exchange energy rates each to one another and σ represents the attenuation.

The above system can be also explained using a similar approach based on the classic mechanics. To that effect, the case of the motion of a spring subject to a damping force was here taken into account, as represented in Figure 3.

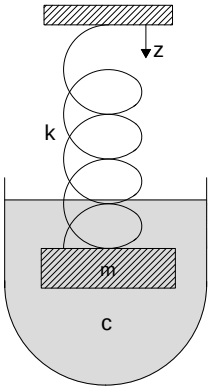

Figure 3. The analogous mechanical system: the motion of an ideal spring subject to a damping force.

In the above scheme, a mass *m* is fastened to a spring with an elastic constant *k*. The spring moves in a fluid that offers a resistive damping force. This is in turn defined by the damping constant *c*. The motion of the mass can be expressed by the following second order differential equation:

$$m\frac{\partial z^2}{\partial t^2} + c\frac{\partial z}{\partial t} + kz = 0 \tag{4}$$

The pulsation ω of such a system can be defined as follows:

$$\omega = \omega_n\sqrt{1-\xi^2} \tag{5}$$

with $\omega_n = \sqrt{k/m}$ being the natural pulsation of the system in stationary conditions, and $\xi = c/c_{cr}$ being the damping factor. c_{cr} is the critical damping coefficient equal to $2\sqrt{km}$. The solutions to Eq. (4) depend on the relationship between *c* and c_{cr}, and they highly influence the speed whereby the energy gets fully dissipated.

In both the above-discussed analogous systems, resonant phenomena are triggered when $\omega = \omega_n$. This occurrence causes a substantial increase of the pulsation amplitude. In the case of systems with low resistance values, this mechanism, although to a lesser extent, is still detectable.

Let us now consider a single ballast aggregate particle subject to the influence of an EM field pulsed around a central frequency with a certain frequency bandwidth. According to the above simplification of the analogous electrical circuit, *L* and *C* depend on the geometric features of the single ballast particle, whereas *R* hinges on the inverse of the electrical conductivity $1/\sigma$ of the medium. Hence, once the dimension of the particle is fixed and σ is known, a particular frequency is expected to generate resonant effects. In the event that this particular

frequency belongs to the bandwidth of the EM pulse, it is therefore expected to observe an amplification of the spectrum at that specific frequency.

In view of the above, the numerical simulation was used to investigate thoroughly the role exerted by *L*, *C* and *R* in the generation of the resonant effects as well as to infer information about the dimension of the ballast aggregates. This allowed analysing the spectral behaviour of different sizes of rock grains that were illuminated by a known pulsed EM field.

4. Numerical simulation

4.1. Single-particle configuration

To validate the theoretical framework of Section 3, a number of numerical simulations were developed. A bi-dimensional scenario was built using the finite-difference time-domain (FDTD) technique implemented in the numerical simulator package gprMax 2D. The model did not include the physical structure of the antenna. A line of current suspended in the free space represented the source. To reproduce the real conditions, the distance between the emitter TX and the receiver RX was set at 0.30 m. Finally, a circle-shaped target with dielectric properties of a typical limestone material (i.e., $\varepsilon_r = 7;\ \sigma = 0.001\ Sm^{-1}$) was selected to represent the ballast particle, and it was placed 0.80 m below the source. The diameter *D* of the particle was varied between 0.04 m and 0.12 m with incremental steps of 0.01 m. This allowed to include the whole set of particle dimensions that are likely to be found on the track-bed and detected by the resolution of the used GPR system. Finally, the ballast particle and the line source were immersed into perfectly matched layers (PML), to avoid potential edge effects (Figure 4).

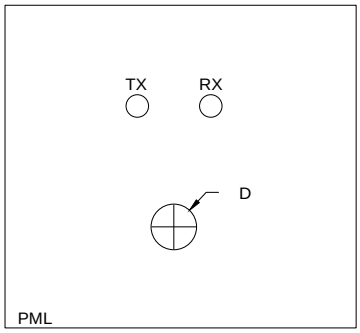

Figure 4. Simulation scenario for a single-particle configuration implemented in the gprMax 2D numerical simulator.

For each of the above-set diameters, an EM pulse was emitted. The central frequency and the time window were set to be 2 GHz and 15 ns, respectively, in accordance with the manufacturer recommendation for this antenna frequency system. The back-received signals were transformed from the time domain to the frequency domain and the corresponding frequency spectra were analysed.

Under ordinary conditions, it is likely to observe a frequency spectrum with an amplitude peak value at the nominal central frequency. Nevertheless, in case the size and the dielectric properties of the ballast aggregate particle define a resonance frequency that belongs to the working bandwidth of the system, it is likely to detect the amplitude peak in the neighbourhood of this frequency. With regard to the above-mentioned case of the analogous electrical circuit, it is expected to detect amplitude peaks at lower frequencies for larger particle diameters. This is related to the fact that the resonance frequency value depends on both L and C, hence, on the grain size of the particle.

Figure 5(a) represents the frequency spectra of single-particle diameters that range between 0.04 m and 0.09 m. For the sake of clarity with the interpretation of the graph, the spectrum amplitude was normalized to the maximum amplitude value of each trace. In accordance with the theory, it was observed that the amplitude peak progressively shifted towards lower values of the frequency as the size of the grain increased. Upper and lower frequency-peak bounds of ~ 2.60 GHz (D = 0.04 m) and ~ 1.10 GHz (D = 0.09 m) were found, respectively.

In the case of particle diameters larger than 0.09 m, the frequency spectra showed peak values centered in the neighborhood of 2 GHz. This frequency value corresponded to the nominal central frequency of the used GPR system (Figure 5(b)).

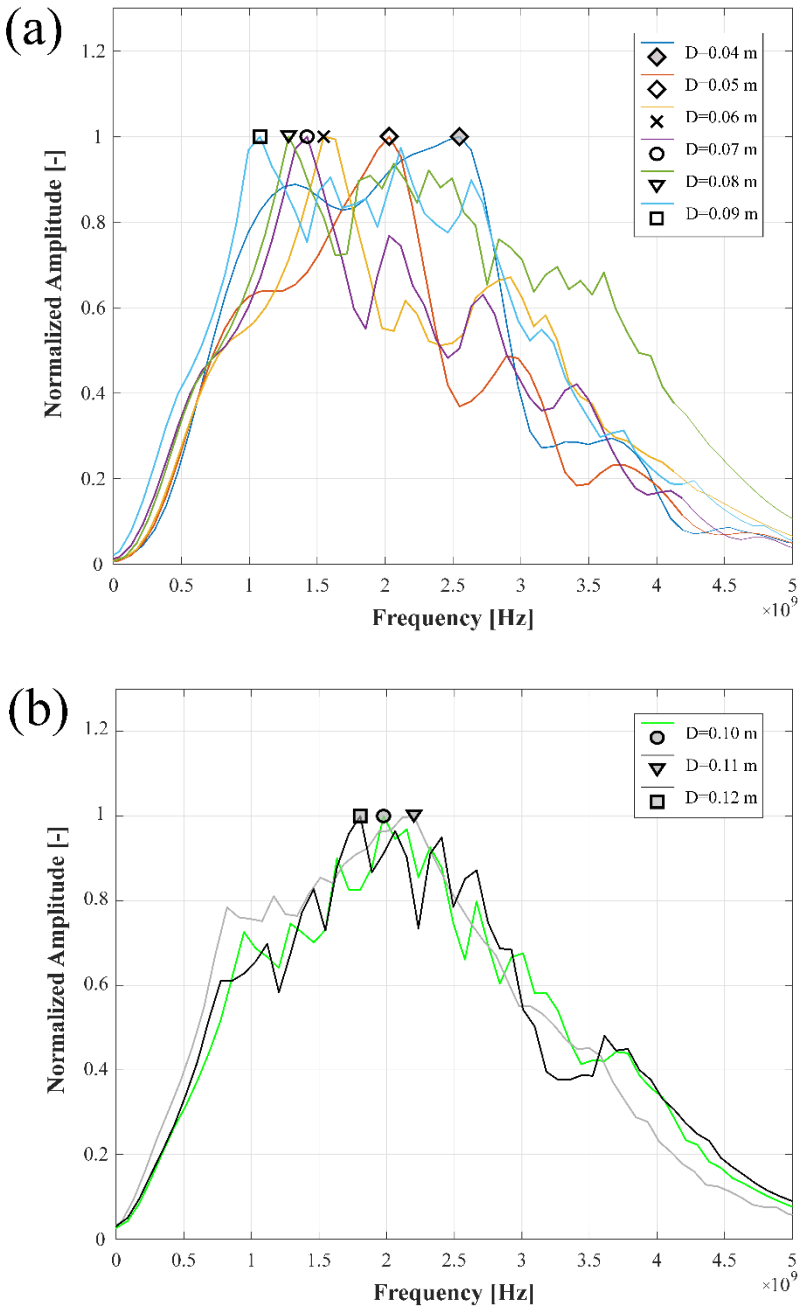

Figure 5. Frequency spectra and corresponding frequency peaks obtained from the single-particle simulations with varying diameters, (a) diameters ranging from 0.04 m to 0.09 m, (b) diameters ranging from 0.10 m to 0.12 m.

4.2. Multi-particle mono-sized configuration

A more complex numerical scenario with a multi-particle configuration of mono-sized ballast aggregates was reproduced and the EM simulation carried out. The main purpose of these simulations was to consider the

actual contribution of the scattering effects and to model the particles arrangement and their interaction close to the real conditions,

To this effect, sets of ten mono-sized round particles were illuminated by the synthetic EM field. The values of the geometric and the electric parameters remained the same as in the single-particle configuration. The relative position of the particles was set randomly to simulate the real-life condition of the ballast aggregates in a track-bed. The mono-sized diameter of each set of particles was increased progressively from 0.04 m up to 0.12 m.

The results of the simulations are shown in Figure 6. As in the case of the single-particle simulations, it was observed a shift of the frequency spectrum peak as a function of the particle grain size. No resonance effects were observed for these particle diameters, in accordance with the theoretical expectations. This was probably due to the fact that nearly no energy was pulsed at lower frequencies than 1 GHz.

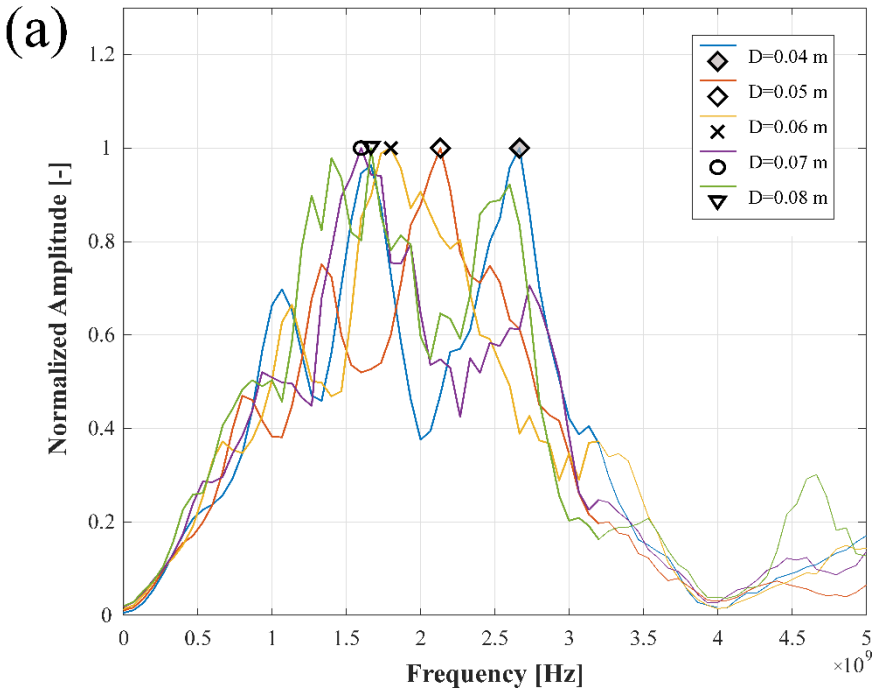

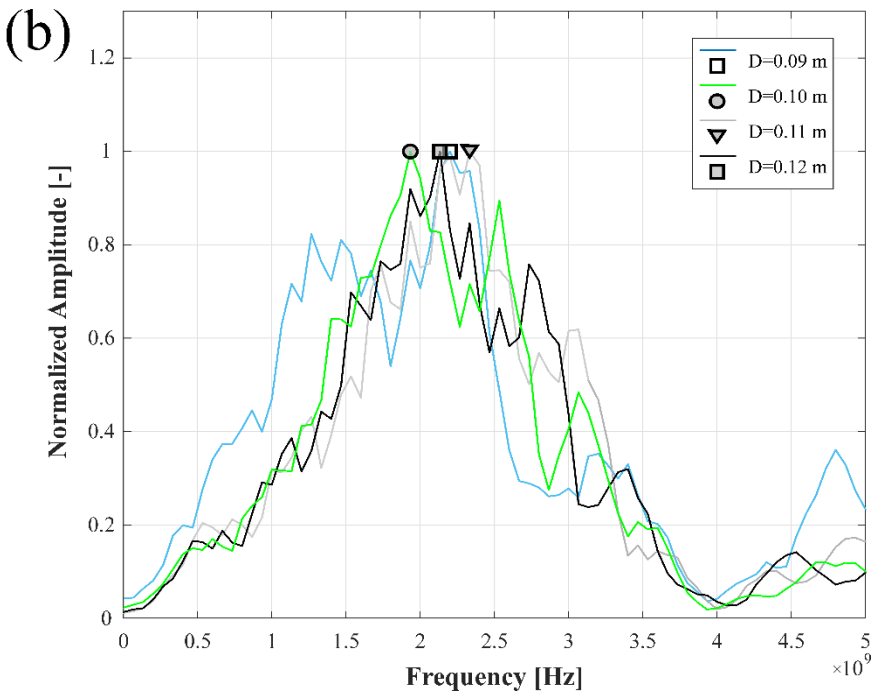

Figure 6. Frequency spectra and corresponding frequency peaks obtained from the multi-particle mono-sized simulations with varying diameters, (a) diameters ranging from 0.04 m to 0.08 m, (b) diameters ranging from 0.09 m to 0.12 m.

4.3. Grading curve configuration

Real-life scenarios of multi-sized grain distributions were subsequently modelled and simulated using reference ballast grading specifications given by the UK Network Rail [25]. In this regard, three grading curves were taken into account for simulation purposes (Figure 7). Curve 1 and Curve 3 represent the upper and lower bounds of the allowed grading, whereas Curve 2 is representative of the intermediate grain size conditions.

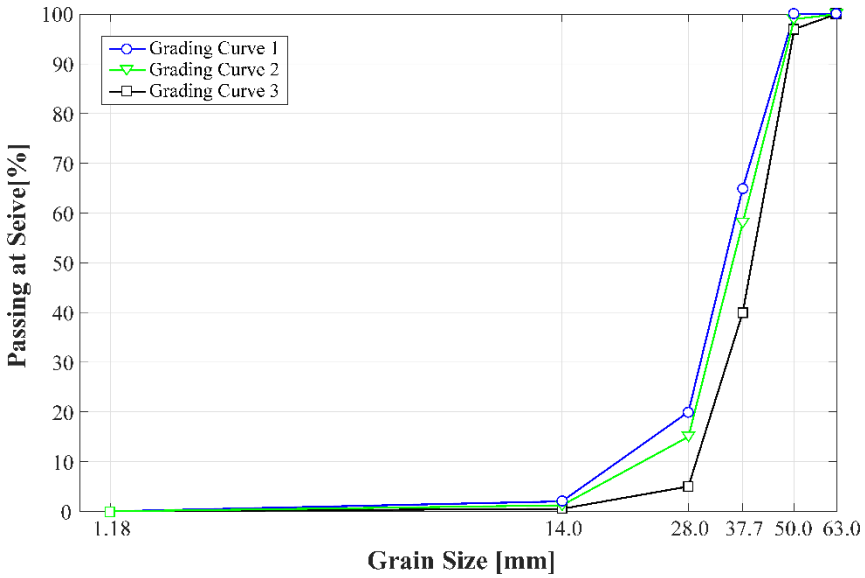

Figure 7. Ballast grading curves [26] of the three real-life ballast scenarios simulated.

A 1.50 m × 0.50 m sized sample made of round-shaped multi-sized ballast particles formed the investigation domain of the ballast aggregates, as shown in Figure 8. For the sake of comparison, both the geometric parameters of the source and the electric properties of the ballast aggregates remained the same as the previous simulations. It is important to emphasize how the dimension of the simulation domain was set up to be representative of the typical thickness of a ballast layer in a rail track-bed [26]. In addition, the dimensions of the numerical domain were designed to comply with the boundary conditions of the experimental set-up built for the GPR investigations made on the real ballast samples in the laboratory environment [27]. With regard to the real sample, the domain was designed according to the beam of radiation of the used GPR system. This allowed avoiding any noise contribution by edge effects, as it will be described later.

According to each of the above-set grain size curves, a number of multi-sized particles were generated by a random numerical process. The particles were placed inside the domain boundaries using the random-sequential adsorption (RSA) paradigm [28, 29]. Once the particles filled the geometric domain, a compaction algorithm was applied to reach compaction conditions close to reality. In more detail, this algorithm was aimed at reproducing the gravitational compaction of the aggregates in a railway ballast layer. To this purpose, downward vertical shifts of the aggregates were considered.

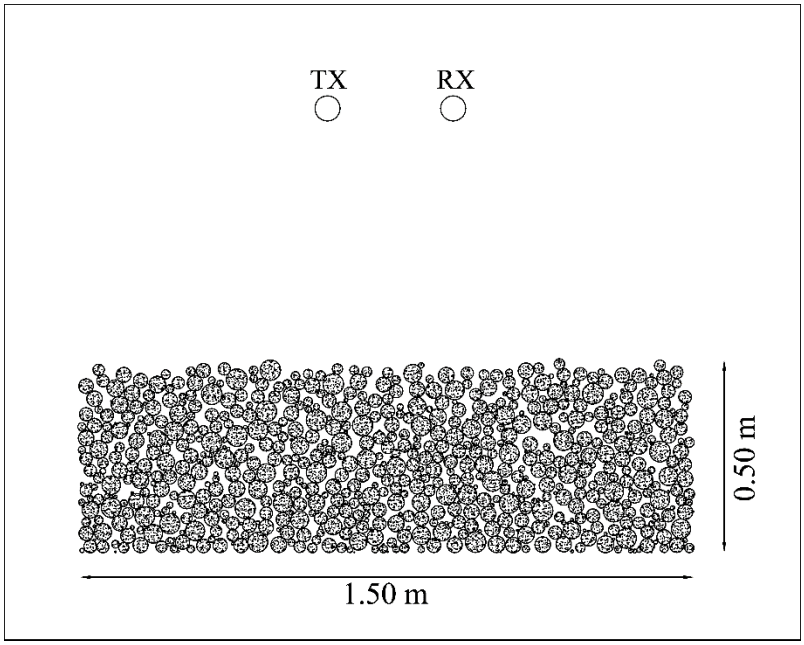

Figure 8. Simulation domain for the multi-sized aggregates distribution as per the information retrieved by one (out of the three) ballast grading curve.

As shown by the grading curves in Figure 7, more than the 80% of the ballast grain size ranges between 28 and 63 mm. To this effect and according to the results of the simulations for the mono-sized multi-particle configurations (i.e., the closest to the multi-sized conditions reproduced by the grading curves here analysed), the above diameters should be related to frequency spectrum peaks comprised between 3.20 GHz and 1.80 GHz, respectively (Figure 6).

In Figure 9, the frequency spectra derived from the simulations with the above three grading curves are shown. In accordance with the spectra trends from the simulations of the single-particle and the mono-sized multi-particle configurations, the results confirmed a shift of the central frequency of the emitted signal as a function of the particle size. In particular, the frequency peak turned out to decrease from 2.80 GHz to 2.53 GHz, as the average size of the grains increased.

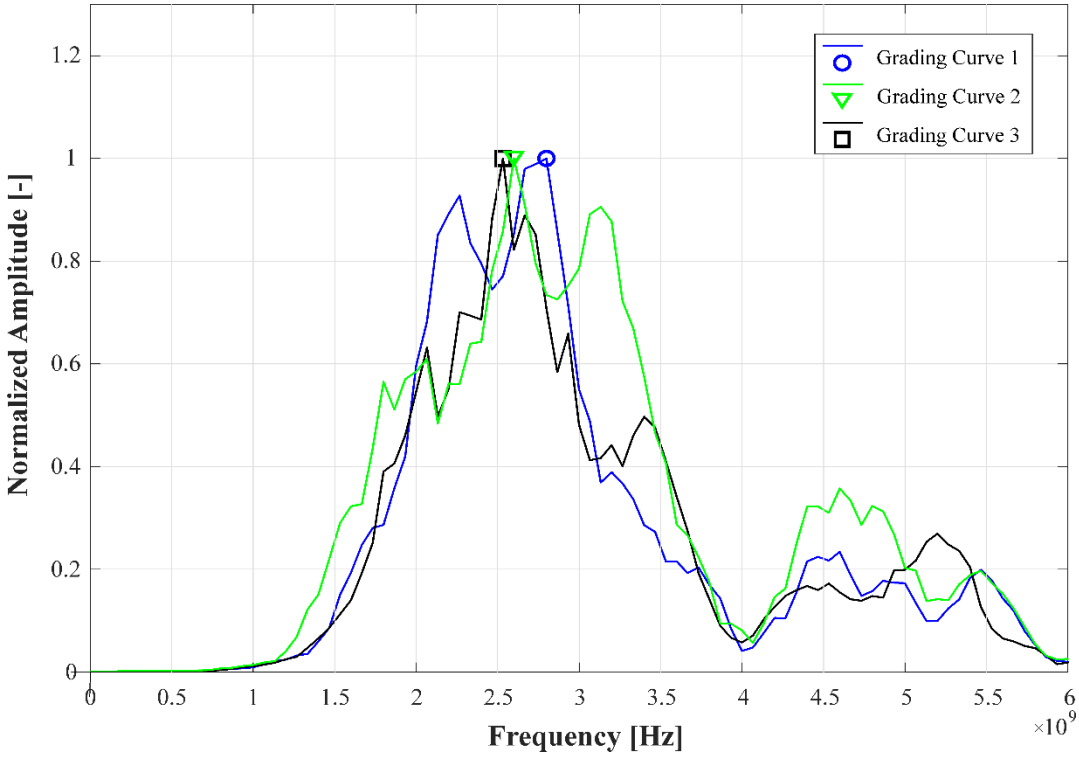

Figure 9. Frequency spectra and corresponding frequency peaks obtained from the simulations with the three grading curves of Figure 7 (1.50 m × 0.50 m sized sample filled with multi-sized round-shaped ballast particles).

For the sake of comparison with the aggregate diameters D_i of the single-particle and the mono-sized multi-particle simulations, the average value $\overline{D}$ of the multi-sized particle diameters was identified for each of the above three curves as distinguishing geometric feature. The value of this parameter was equal to 0.026 m, 0.028 m, and 0.034 m for Curve 1, Curve 2 and Curve 3, respectively.

5. Experimental testing

The real tests were carried out in the laboratory to underpin the theoretical assumptions discussed in Section 3 and verified numerically in Section 4.

In this regard, a square-based methacrylate container was filled with coarse-grained limestone material (Figure 10), typically used for the construction of ballasted track-beds. The GPR data were collected using a 2GHz horn antenna, in accordance with the central frequency used for the simulations in Section 4. The antenna was suspended in the air at 0.40 m above the centroid of the container. The dimensions of the container were 1.50

m length × 1.50 m width × 0.50 m height, according to the dimensions of the real-scale simulation domain shown in Figure 8.

Figure 10. Side view of the methacrylate container filled with limestone railway ballast.

The ballast aggregates used in the tests were composed of coarser grains with dimensions ranging between 0.04 m and 0.09 m. To define an equivalent parameter *D'* representative of the aggregates diameter, the actual ballast aggregates were assumed as ellipsoids. Thereby, the maximum and minimum dimensions of n = 200 randomly sampled aggregates were measured in the laboratory with a caliper [30]. For each i^{th} particle of the sampled population of ballast aggregates, the average diameter D_i' between these two reference dimensions was computed. Consequently, the equivalent value *D'* was calculated as follows:

$$D' = \frac{\sum_{i=1}^{n=200} D_i'}{n} \quad (6)$$

The above parameter, assumed for the whole grain size distribution, was equal to 0.07 m.

To evaluate the influence on the signal frequency spectrum of the multi-sized particles arrangement in the container, three different scenarios of aggregates arrangement were manufactured in the laboratory by filling and emptying out the container three times. No compaction procedure was applied using external forces. A gravitational compaction was ensured by the own weight of the aggregates. For each of the above scenarios, the GPR data were collected using the 2GHz antenna system. The corresponding frequency spectra are shown in Figure 11.

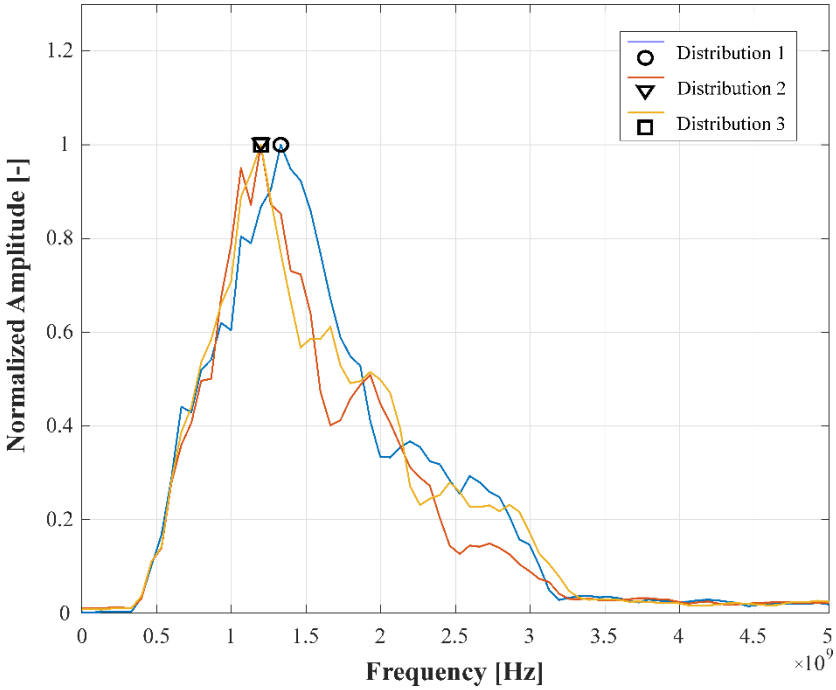

Figure 11. Frequency spectra and corresponding frequency peaks related to the real GPR data collected in the laboratory for the three scenarios of multi-sized ballast particles arrangement in the container.

As it can be seen from the Figure 11, the values of the frequency peak ranged between 1.20 GHz and 1.33 GHz. Thereby, it was proved that the peak shifted away from the 2GHz nominal frequency. Overall, the spectral behaviour showed a shift towards lower frequencies. This was consistent with the larger average dimension of the ballast aggregates. Moreover, the limited variation of the frequency peak value among the three investigated scenarios proved a minor influence of the spatial distribution of the particles on the value of the resonant frequency. This remark has validity when a multi-sized coarse-grained material (such as the railway ballast aggregates used in the above laboratory tests) is considered.

6. Discussion

In accordance with the theoretical assumptions of Section 3, the spectral analyses derived from both the simulation cases and the laboratory tests confirmed a shift of the frequency spectrum peak as a function of the dimension of the aggregate particles. As far as the single-particle and mono-sized multi-particle configurations are concerned, a decreasing trend of the peak of the frequency spectra for increasing values of the diameter was demonstrated (Figure 5 and Figure 6). The main differences between such two tested configurations were

found in the shape of the spectra, which were more irregular in the multi-particle case due to the scattering and the surface effects. In addition, the range of applicability of the resonance method for the fixed bandwidth was slightly different. It has varied from the 0.04 m ÷ 0.09 m range for the single-particle configuration (Figure 5(a)), to the 0.04 m ÷ 0.08 m range for the mono-sized multi-particle configuration (Figure 6(a)). Indeed, in the multi-particle case, the maximum peak was still detected in a neighbourhood of ~ 2 GHz, although for D = 0.09 m it was possible to notice a major amplitude peak at ~ 1.5 GHz.

Finally, a number of more complex simulations (i.e., sets of multi-sized aggregates derived from three reference grading curves) and GPR laboratory tests (i.e., multi-sized real aggregates of ballast) were performed on comparable test domains. Apart from the simulated and the real figures of the above tests, the main difference was related to the size of the grains in the sample, which were smaller in the simulated case (Figure 9) than in the laboratory tests (Figure 11). On the other hand, the common multi-sized particle distribution led to define in both cases a (similar) reference geometric parameter to relate with the frequency spectrum peak. Thereby, an average radius $\overline{D}$ (for the simulations) and an equivalent diameter D' (for the real tests) were set.

7. Experimental-based modelling

The modelling of the grain size of the ballast particles and the frequency spectrum peak of the collected GPR signal was developed to provide a relationship between these two parameters within the allowed frequency bandwidth bounds. To that effect, Figure 12 shows the negative exponential relationship found using the data from the single-grain and the mono-sized multi-grain simulations:

$$f_p = \alpha e^{-\beta D^*} \tag{7}$$

where f_p is the frequency of the spectrum peak, D^* is the aggregate diameter, and [α, β] are fitting parameters dependent on the specific configuration. The mean squares fitting curves were characterised by high correlation coefficients R^2, as listed in Table 1.

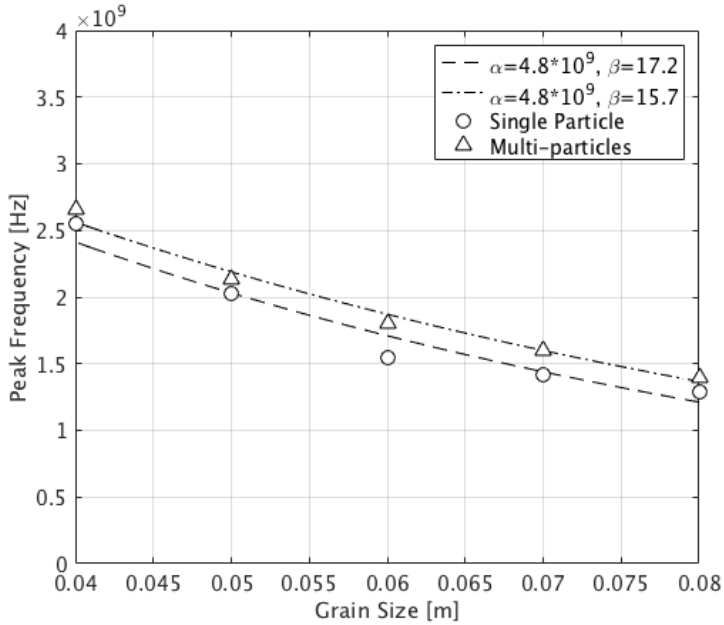

Figure 12. Exponential trend lines fitting the frequency peak against the grain size data collected for the single-particle (circular markers) and the mono-sized multi-particle (triangular markers) configurations.

Table 1. Regression coefficients in Equation (7).

Configuration (mono-sized grading)	α	β	R^2
Single-particle	4.8×10^9	17.20	0.946
Multi-particle	4.8×10^9	15.70	0.983
Average regression values	4.8×10^9	16.45	0.964

To analyse the applicability of the above relationship over the multi-particle arrangement of ballast particles with multi-sized grading (i.e., the real-life like condition), let us now express Eq. (7) as a function of D^*:

$$D^* = -\left(\ln \frac{f_p}{\alpha}\right) \cdot \beta^{-1} \tag{8}$$

Working out i) the regression coefficients α and β found by the mono-sized multi-particle simulations (Table 1) and ii) the frequency peak values computed for the three grain size distributions in Section 4.3 (Figure 8) into Eq. (8), it was possible to define a characteristic diameter D^* for each multi-sized grain distribution, as reported in Table 2.

Table 2. Frequency and geometric parameters of the three railway ballast grading curves (1.50 m × 0.50 m sized sample filled with multi-sized round-shaped ballast particles).

Grading curve	f_p [GHz]	D^*[cm]	$\overline{D}$[cm]	ζ [%]
1	2.80	3.30	2.60	21.2
2	2.53	3.90	3.40	12.8
3	2.60	3.80	2.80	26.3

The comparison between the characteristic diameter D^* (calculated from the proposed numerical-based modelling) and the average diameter $\overline{D}$ (assessed from the diameters of the whole set of synthetic round-shaped ballast aggregates in the simulation domain), proved that an average geometric feature was not fully representative of the size distribution of the ballast matrix. Indeed, the percentage errors ζ to the values of D^* between $\overline{D}$ and D^* are greater than 25% (worst case). This might be due to the different shifting trend of the frequency spectrum peak observed in the multi-sized particle scenarios (Figure 9), compared to the case of mono-sized particle arrangements (Figure 6). More complex scenarios in terms of multi-sized grading provided a narrower range of variation for the frequency spectrum peak.

Following the same approach with the real GPR data collected from the laboratory tests, it was possible to compare the characteristic diameter D^*, computed by Eq. (8), with the value of the equivalent diameter D', assessed by Eq. (6). The results are included in Table 3. In this case, it is worth noting that the value of the equivalent diameter D' was a constant, since the same aggregates were used for manufacturing the three scenarios of ballast particles arrangement.

Table 3. Frequency and geometric parameters of the three scenarios of multi-sized ballast particles arrangement in the container (model application to the real case).

Scenario	f_p [GHz]	D^*[cm]	D' [cm]	ζ [%]
1	1.20	8.70	7.00	19.5
2	1.20	8.70	7.00	19.5
3	1.33	8.00	7.00	12.5

The elliptical approximation used for the assessment of D' showed better performances, with percentage errors ζ lower than 20%. As in the multi-sized simulation case, it was noticed that the experimental model tended to underestimate the value of the equivalent diameter.

8. Conclusion and future perspectives

In this work, the spectral behaviour of 2GHz ground-penetrating radar (GPR) signals collected under a multi-stage process in terms of ballast grain size was analysed. Furthermore, the modelling of "critical" geometric features of the ballast aggregates and the peak of the frequency spectrum was developed. The study reported on the possibility to retrieve relevant information about the grain size of the ballast aggregates in the rail subsurface layers and the possible segregation of the aggregates under heavy cyclic loading. To that effect, a bottom-up methodology for the assessment of railway ballast using ground-penetrating radar (GPR – 2 GHz horn antenna) was developed. The theoretical framework was underpinned by the case of "analogous" electrical and mechanical systems, which were representative of the "ballast aggregates condition" (i.e., the geometric features and the arrangement of the aggregates) against the EM field interaction. To validate the theoretical assumptions, a number of finite-difference time-domain (FDTD) simulations of the GPR signal and actual GPR tests in the laboratory were carried out. These tests allowed investigating thoroughly the propagation and the scattering of the EM waves in a ballast layer of a typical rail track-bed. The spectral response of the GPR data in the frequency domain was first analysed in the case of mono-sized single- and multi-particle configurations of round-shaped ballast aggregates with different diameters and electric properties consistent with literature references. Afterwards, the numerical scenario was rendered more complex by using multi-sized particles under compaction conditions close to reality. To that effect, reference ballast grading specifications given by a railway network operator were taken into account and the random-sequential adsorption (RSA) paradigm was applied in combination with the FDTD technique. Overall, the spectral analyses from both the simulation cases and the laboratory tests confirmed a shift of the frequency spectrum peak as a function of the dimensions of the aggregate particles, as it was expected by the theoretical assumptions. In this regard, it was proved a decreasing trend of the peak of the frequency spectrum as the value of the diameter increased in the 0.04÷0.09 m range. The simulations from the simplified mono-sized multi-particle scenarios turned out to provide more irregular shapes of the frequency spectra than the single-particle simulations. In addition, the range of applicability of the resonance method was proved to be slightly different among the single and the multi-particle simulations. This was likely due to the scattering and the surface effects that arose from the EM wave propagation in the multi-particle model. With regard to the real-scale simulations

and the laboratory investigations, comprehensive geometric parameters (i.e., equivalent diameters of the aggregates) representative of the grain size distributions of the ballast were set using a circular and an elliptical approximation of the aggregates shape, respectively. Hence, experimental relationships between the aggregate diameter and the peak of the frequency spectrum were found from the results of the single- and multi-particle simulations. The modelling of the multi-particle simulation scenarios was used to underpin the proposed theoretical assumptions and to infer information about the grain size of the ballast aggregates from the real-scale simulations and the laboratory (actual) GPR tests. Overall, the experimental model tended to underestimate the computed equivalent diameter. In addition, the elliptic approximation used for the shape of the ballast aggregates (i.e., the case of the laboratory GPR tests) performed better, with percentage errors lower than 20%.

Further theoretical investigations might be aimed at increasing the reliability of the proposed frequency-based methodology by using stepped-frequency continuous-wave (SFCW) GPR systems. In addition, the effectiveness of the model could be tested against different conditions of fouling, e.g., in the presence of fine material that rises from the foundation level and fills the inter-particle voids. To that effect, dedicated simulations and real-life tests could be developed following the methodology discussed in this study.

Acknowledgements

The authors express their thanks to Mr. Daniele Pirrone, from Roma Tre University, for his help and advice in the research; Mr. Spartaco Cera, from Roma Tre University, for the technical assistance in the laboratory surveys. Special thanks to IDS Georadar for supplying part of the GPR systems, and Clax Italia s.r.l. for manufacturing the methacrylate container. This work has also benefited from the network activities carried out within the EU funded COST Action TU1208 “Civil Engineering Applications of Ground Penetrating Radar. ”

References

1. Indraratna B. 1st Ralph Proctor Lecture of ISSMGE. Railroad performance with special reference to ballast and substructure characteristics. Transport Geotech 2016;7:74–114.
2. Selig ET, Waters JM. Track geotechnology and substructure management. London: Thomas Telford; 1994.
3. Clark M, McCann DM, Forde MC. Infrared thermographic investigation of railway track ballast. NDT&E Int 2002;35(2):83–94.
4. Anbazhagan P, Buddhima I, Amarajeevi, G. Characterization of clean and fouled rail track ballast subsurface using seismic surface survey method: model and field studies. J Test Eval 2011;39(5):831–841.
5. Donohue S, Gavin K, Tolooiyan A. Geophysical and geotechnical assessment of a railway embankment failure. Near Surf Geophys 2001;9(1):33–44.
6. Hugenschmidt J. Railway track inspection using GPR. J Appl Geophys 2000;43:147–155.
7. Roberts R, Schutz A, Al-Qadi IL, Tutumluer E. Characterizing railroad ballast using GPR: recent experiences in the United States. In: Proceedings of the 4th international workshop on advanced ground penetrating radar (IWAGPR 2007), Naples, Italy (2007).
8. Railway Track and Structures Magazine, June 1985.
9. Daniels DJ. Ground Penetrating Radar, 2nd ed. London: The Institution of Electrical Engineers; 2004.
10. Clark MR, Gillespie R, Kemp T, McCann DM, Forde MC. Electromagnetic properties of railway ballast. NDT&E Int 2001;34(5):305–311.
11. Sussmann TR, O'Hara KR, Selig ET. Development of material properties for railway application of ground penetrating radar. In: Proceedings of the society of photo-optical instrumentation engineers (SPIE); 2002 vol. 4758.
12. Tosti F, Benedetto A, Calvi A, Bianchini Ciampoli L. Laboratory investigations for the electromagnetic characterization of railway ballast through GPR. In: Proceedings of the 16th international conference of ground penetrating radar (GPR 2016), Hong Kong (2016).
13. Fontul S, Fortunato E, De Chiara F. Evaluation of ballast fouling using GPR. In: Proceedings of the 15th international conference on ground penetrating radar (GPR 2014), Bruxelles, Belgium (2014). p. 418-422.

14. Anbazhagan P, Naresh Dixit PS, Bharatha TP. Identification of type and degree of railway ballast fouling using ground coupled GPR antennas. J Appl Geophys 2016;126:183–190.
15. Roberts R, Rudy J, Al-Qadi IL, Tutumluer E. Railroad ballast fouling detection using ground penetrating radar – a new approach based on scattering from voids. In: Proceedings of the ninth european conference on NDT (ECNDT 2006), Berlin, Germany (2006). p. 1–8.
16. Forde MC, De Bold R, O'Connor G, Morrissey JP. New analysis of ground penetrating radar testing of a mixed railway trackbed. Transportation Research Board Annual Meeting (2010).
17. Leng Z, Al-Qadi IL. Railroad ballast evaluation using ground-penetrating radar. Transport Res Rec 2010;2159:110–117.
18. Shao W, Bouzerdoum A, Phung SL, Su L, Indraratna B, Rujikiatkamjorn C. Automatic classification of ground-penetrating-radar signals for railway-ballast assessment. IEEE T Geosci Remote 2011;49(10);3961–3972.
19. Xiao J, Liu L. Multi-frequency GPR signal fusion using forward and inverse S-transform for detecting railway subgrade defects. In: Proceedings of the 8th international workshop on advanced ground penetrating radar (IWAGPR 2015), Florence, Italy (2015).
20. Zhang Q, Gascoyne J., Eriksen A. Characterisation of ballast materials in trackbed using ground penetrating radar: Part 1. In: Proceedings of the 5th IET Conference on Railway Condition Monitoring and Non-Destructive Testing (RCM 2011), Derby, United Kingdom (2011). p. 1–8.
21. Xiao J, Liu L. Multi-frequency GPR signal fusion using forward and inverse S-transform for detecting railway subgrade defects. In: Proceedings of the 8th international workshop on advanced ground penetrating radar (IWAGPR 2015), Florence, Italy (2015).
22. Benedetto A, Tosti F, Bianchini Ciampoli L, Calvi A, Brancadoro MG, Alani AM. Railway ballast condition assessment using ground-penetrating radar – an experimental, numerical simulation and modelling development. Constr Build Mater 2016;140:508–520.
23. Liu L, Li Z, Arcone S, Fu L, Huang Q. Radar wave scattering loss in a densely packed discrete random medium: numerical modeling of a box-of-boulders experiment in the Mie regime. J Appl Geophys 2013;99:68–75.

24. Giannopoulos A. Modelling ground penetrating radar by GprMax. Constr Build Mater 2005;19(10):755–762.
25. Network Rail. Railway ballast & stoneblower aggregate. NR/L2/TRK/8100 Issue 4, 2009.
26. Roberts R, Al-Qadi IL, Tutumluer E, Boyle J, Sussmann TR. Advances in railroad ballast evaluation using 2 GHz horn antennas. In: Proceedings of the 11th international conference on ground penetrating radar, Columbus, USA (2006).
27. Roberts R, Al-Qadi IL, Tutumluer E, Kathage A. Ballast fouling assessment using 2 GHz horn antennas - GPR and ground truth comparison from 238 km of track. In: Proceedings of the 9th international railway engineering conference, London, UK (2007).
28. Benedetto A, Umiliaco A. Evaluation of hydraulic permeability of open-graded asphalt mixes using a full numerical simulation. J Mater Civil Eng 2014;26(4):599-606.
29. Benedetto A, Tosti F, Bianchini Ciampoli L, Pajewski L, Pirrone D, Umiliaco A, Brancadoro MG. A simulation-based approach for railway applications using GPR. In: Proceedings of the 2016 International Conference of Ground Penetrating Radar (GPR 2016), Hong Kong (2016).
30. EN 933-4:2008. Tests for geometrical properties of aggregates - Part 4: determination of particle shape - shape index. European Committee for Standardization, 2008.